Mixed Main Group Transition Metal Clusters: Reactions of $[Ru_3(CO)_{10}(\mu\text{-dppm})]$ with Ph_3SnH

Md. Mehedi Mahabub Khan [a], Shishir Ghosh [a], Graeme Hogarth [b], Derek A. Tocher [c], Michael G. Richmond [d], Shariff E. Kabir [a, e, *], Herbert W. Roesky [e, *]

[a] *Department of Chemistry, Jahangirnagar University, Savar, Dhaka 1342, Bangladesh*

[b] *Department of Chemistry, King's College London, Britannia House, 7 Trinity Street, London SE1 1DB, UK*

[c] *Department of Chemistry, University College London, 20 Gordon Street, London WC1H OAJ, UK*

[d] *Department of Chemistry, University of North Texas, Denton, Texas 76203, USA*

[e] *Georg-August University, Institute of Inorganic Chemistry, 4, D-37077 Göttingen, Germany*

*Corresponding authors. E-mail addresses: skabir_ju@yahoo.com (S. E. Kabir), hroesky@gwdg.de (H.W. Roesky)

ABSTRACT

Novel dppm-ligated ruthenium-tin clusters have been prepared from the reaction of $[Ru_3(CO)_{10}(\mu\text{-dppm})]$ with Ph_3SnH. At room temperature and in the presence of Me_3NO, $[Ru_3(CO)_9(SnPh_3)(\mu\text{-dppm})(\mu\text{-H})]$ (**1**) is produced from the formal loss of CO and Sn-H bond oxidative-addition.Treatment of **1** with a further two equivalents of Ph_3SnH (in the presence of Me_3NO) gave $[Ru_3(CO)_7(SnPh_3)_2(\mu\text{-}SnPh_2)(\mu\text{-dppm})(\mu\text{-H})(\mu_3\text{-H})]$ (**2**) which results from both Sn–H and Sn–C bond scission and contains two different hydride environments (μ and μ_3) and a $\mu\text{-}SnPh_2$ moiety. Cluster **2** has 48 CVE (cluster valence electron) with three formal ruthenium-ruthenium bonds; two of those are very long and fall at the extreme end of distances attributed to ruthenium-ruthenium bonds. Thermolysis of **2** at 66 ^oC liberates benzene to give $[Ru_3(CO)_8(SnPh_3)(\mu\text{-}SnPh_2)(\mu_3\text{-}SnPh_2)(\mu\text{-dppm})(\mu\text{-H})]$ (**3**). DFT calculations confirm that the hydride bridges one of the Ru-μ-$SnPh_2$ bonds in **3**. The solid-state structures of **2** and **3** have been determined by X-ray crystallography, and the bonding and ligand distribution have been investigated by DFT studies. The geometry-optimized structures are consistent with the solid-state structures.

Keywords: Triruthenium clusters, Triphenyltin activation, Diphosphine ligand, DFT

1. Introduction

Polynuclear metal carbonyl complexes containing tin can serve as precursors to bi- and multi-metallic nanoscale heterogeneous catalysts that exhibit extremely high activity and superior selectivity for certain types of hydrogenation and dehydrogenation reactions when anchored on oxide supports [1-4]. The enhanced catalytic activity extant in such systems is attributed to tin's ability to modify the electronic properties and particle size distribution of the heterogeneous transition metal catalyst/nanoparticle [4-6]. Consequently, several methods have been developed to incorporate tin into the coordination sphere of polynuclear metal carbonyl complexes. The most widely used method is the oxidative addition of organotin hydrides (Sn-H) to metal cluster complexes as exemplified by the work of Adams [7-9] and Cabeza [10,11]. A second method is the oxidative addition of other (organo)tin-element bonds (Sn-C, Sn-S and Sn-N) to such cluster complexes [12-15]. Recently, Cabeza et al. also shown that stannylenes stabilized by organic amides can be easily incorporated into the coordination sphere of polynuclear metal carbonyl complexes via direct reaction between them [16].

Empirically, the reaction of unsupported metal carbonyl clusters with organotin hydrides or other tin sources is typically accompanied by the formation of lower nuclearity products produced by cluster degradation [9,12]. Since it has been established that the diphosphine bis(diphenylphosphino)methane (dppm) can stabilize the trimetallic core of Group 8 clusters with respect to degradation, we have employed triruthenium and triosmium clusters $[M_3(CO)_{10}(\mu\text{-dppm})]$ (M = Ru, Os) to help stabilize the metallic polyhedron from unwanted fragmentation during the incorporation of tin. Stoichiometrically-controlled addition of tin to $[M_3(CO)_{10}(\mu\text{-dppm})]$ potentially facilitates the preparation of tin derivatives in a systematic fashion, which in turn allows for reproducible molecular heterogeneity of M_xSn_y nanoparticle-derived catalysts. Moreover, important mechanistic insight associated with the early activation steps of the ancillary tin ligands at a trinuclear cluster can be investigated as the catalyst precursor transforms to the alloy catalyst/nanoparticle [13,16,17]. We have previously reported our results from the reactions of $[Os_3(CO)_{10}(\mu\text{-dppm})]$ with Ph_3SnH and Ph_3GeH which showed that the dppm ligand successfully prevented cluster fragmentation [13a,18]. Herein we report our findings on related reactions $[Ru_3(CO)_{10}(\mu$-

dppm)] with Ph_3SnH which gives rise to some novel ruthenium-tin clusters, the structure and bonding of which have been investigated by DFT calculations.

2. Results and discussion

Treatment of $[Ru_3(CO)_{10}(\mu\text{-dppm})]$ with excess Ph_3SnH in the presence of Me_3NO at room temperature affords the new clusters $[Ru_3(CO)_9(SnPh_3)(\mu\text{-dppm})(\mu\text{-H})]$ (**1**) and $[Ru_3(CO)_7(SnPh_3)_2(\mu\text{-}SnPh_2)(\mu\text{-dppm})(\mu\text{-H})(\mu_3\text{-H})]$ (**2**) in 45 and 24% yield, respectively, after chromatographic separation and workup (Scheme 1). Independent control experiments subsequently revealed that **1** serves as the precursor to **2** when treated with Ph_3SnH under comparable reaction conditions, thus confirming the sequential formation of **1** and then **2** starting from $[Ru_3(CO)_{10}(\mu\text{-dppm})]$. Under no conditions could a product containing two tin atoms (i.e. a Ru:Sn ratio of 3:2) be isolated. Refluxing $[Ru_3(CO)_{10}(\mu\text{-dppm})]$ and Ph_3SnH in THF also gave **1** and **2** together with a third product, $[Ru_3(CO)_8(SnPh_3)(\mu\text{-}SnPh_2)(\mu_3\text{-}SnPh_2)(\mu\text{-dppm})(\mu\text{-H})]$ (**3**), which was isolated in 30% yield. Thermolysis of **1** and **2** in THF in the presence of excess Ph_3SnH also furnished **3** (Scheme 1) and we also confirmed that, while **2** undergoes transformation to **3** when refluxed in THF in the absence of added Ph_3SnH, the reaction is accompanied with extensive decomposition.

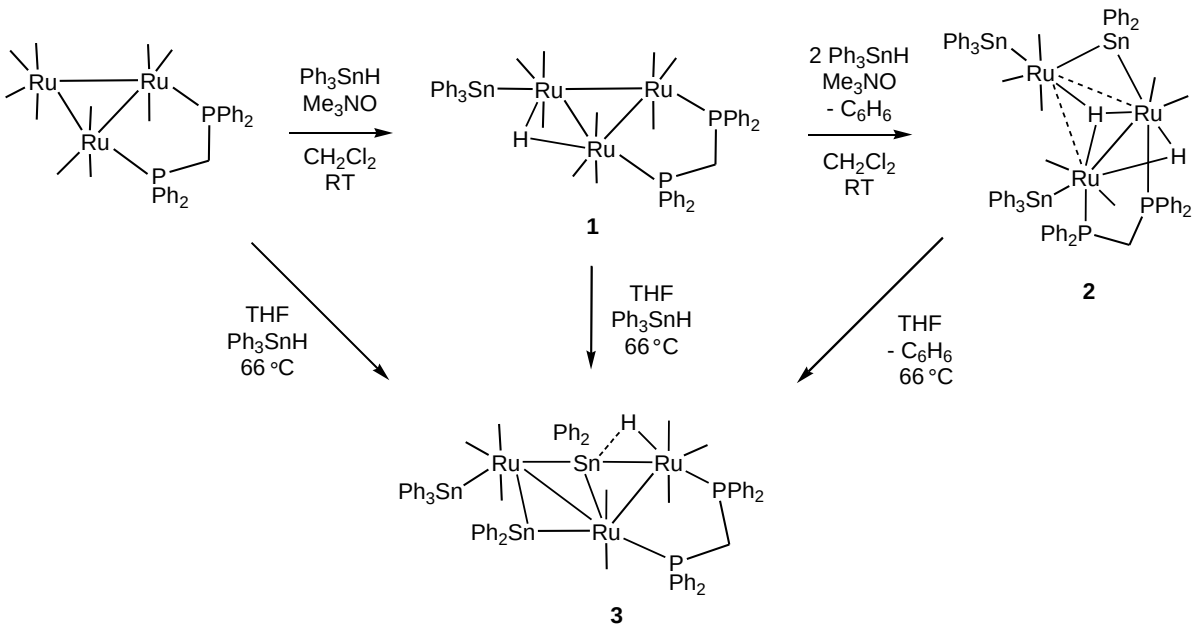

Scheme 1. Products isolated from the reaction of $[Ru_3(CO)_{10}(\mu\text{-dppm})]$ with Ph_3SnH.

Cluster **1**was characterized by analytical and spectroscopic methods. The FAB mass spectrum shows a molecular ion at *m/z* 1291 along with further ions due to the sequential loss of nine carbonyls. The ^{1}H NMR spectrum displays an upfield doublet at δ -18.32 (J_{PH} 31.6 Hz) for a bridging hydride, the coupling pattern showing that it does not span the dppm-bridged Ru-Ru bond. The spectrum also shows a virtual triplet at δ 4.55 (J 10.8 Hz) for the methylene moiety of the dppm ligand, in addition to aryl resonances from δ 7.82-7.07 ascribed to the dppm and Ph_3Sn ligands. The $^{31}P\{^{1}H\}$ NMR spectrum exhibits two broad singlet at δ 7.9 and 6.7 for the dppm ligand instead of two doublets as expected due to the non-symmetrical binding of this ligand. We suggest that the molecule is fluxional in solution at ambient temperatures due to the movement of triphenyltin and hydride ligands (Chart S1 in supplementary information) as observed in related complexes such as $[Os_3(CO)_9(SnPh_3)(\mu\text{-dppm})(\mu\text{-H})]$ [13a] and $[Os_3(CO)_9(SiR_3)(\mu\text{-dppm})(\mu\text{-H})]$ (R = Et, Ph) [19]. Most probably for the same reason ^{119}Sn satellites were not observed in the hydride signal at room temperature. In order to arrest this fluxional process we lowered the temperature, but were unable to see the ^{119}Sn satellites even at 213 K (Fig. S10). The two broad singlets observed in the $^{31}P\{^{1}H\}$ NMR spectrum at room temperature gradually sharpen as the temperature was lowered, but we did not observe the expected splitting even at 213 K (Fig. S12). The IR spectrum of **1** exhibits carbonyl absortions within the range 2079-1923 cm^{-1} and the pattern of this spectrum is also quite similar to that observed for $[Os_3(CO)_9(SnPh_3)(\mu\text{-dppm})(\mu\text{-H})]$ [13a]. The osmium analogue $[Os_3(CO)_9(SnPh_3)(\mu\text{-dppm})(\mu\text{-H})]$ [13a] was strucrually characterized which confirmed the disposition of the hydride and Ph_3Sn ligands relative to the dppm-tethered Os-Os bond. The large Ph_3Sn ligand occupies one of the two equatorial sites at the adjacent ruthenium centre with the hydride located at the sterically least crowded equatorial site *cis* to the Ph_3Sn group.

The locus preference for the disposition of the hydride and Ph_3Sn ligands relative to the bridging dppm ligand in **1** was investigated by density functional theory (DFT). Two structures were optimized (**A** and **A_alt**), each possessing an edge-bridged hydride and an equatorially situated Ph_3Sn ligand that was oriented either *cis* or *trans* to the hydride (Fig. 1). They differ by 2.2 kcal/mol (ΔG) in favour of the *cis* isomer **A**, supporting the anticipated structure for cluster **1**. We also computed the natural charges and Wiberg bond index (WBI) for the different Ru-Ru, Ru-Sn, and Ru-H bonds in **A** (Table 1). The charges on the ruthenium atoms are all negative and range from -1.40 (Ru_2) to -1.58 (Ru_3), and the mean

charge for the two phosphorus atoms is 1.34. The computed charges for the tin and hydride ligands are both positive (1.79 and 0.13, respectively). The computed distance of 3.1236 Å for the Ru_1-Ru_3bond is 0.18 Å longer than the mean distance for the other two Ru-Ru bonds in **A**, and this is reflected in the Wiberg bond indices, which serve as a measure of bond strength. The longer hydride-bridged Ru_1-Ru_3 bond exhibits a Wiberg index that is nearly 60% shorter than the WBIs of other two Ru-Ru bonds. The computed WBIs are consistent with the structure of **A** and the trends in bond lengths reported by us for related metal clusters [13b,20].

Place Figure 1 and Table 1 Here

The identity of **2** and **3** could not be ascertained from spectroscopic data and accordingly we carried out single crystal X-ray diffraction analyses to establish their molecular architecture. The structure of **2** is depicted in Fig. 2, whose caption also exhibits selected bond lengths and angles. The molecule results from the formal addition of three equivalents of Ph_3SnH to the triruthenium centre, followed by further cleavage of a tin-phenyl bond probably extruded as benzene. There are two long and one short ruthenium-ruthenium vectors. The Ru(1)-Ru(2) distance of 2.9439(3) Å is bridged by the dppm ligand and is consistent with a single-bond designation. The Ru(2)-Ru(3) [3.2355(5) Å] and Ru(1)-Ru(3) [3.3992(7) Å] distances are considerably longer than the dppm-bridged metallic edge but do fall within the van der Waals radii for two ruthenium atoms [23]. These are best viewed as weak Ru-Ru single bonds since the cluster has a total electron count of 48 [24]. Examples of polynuclear ruthenium clusters with Ru-Ru bond(s) exceeding 3.10 Å include $[\{(\eta^6\text{-}C_6Me_6)_2Ru_2H_2(CH_2Cl_2)\}RuB_{10}H_8(OEt)_2]$ [25], $Ru_5Pt_5(CO)_{18}(COD)_2(\mu_3\text{-}H)_2$ [23], $[\{Ru_3H(pyS)(CO)_7\}_3]$ [24], and $[AuRu_6(\mu_3\text{-}H)(\mu\text{-}O{:}\mu\text{-}C{:}\eta^6\text{-}OC_6H_3OMe\text{-}4)(CO)_{16}(PPh_3)]$ [26].

Place Figure 2 Here

The two Ru-P bond distances in **2** are symmetric [Ru(1)–P(1) 2.3825(7) and Ru(2)–P(2) 2.3996(6) Å] and the seven CO groups exhibit bond distances and angles unremarkable relative to ruthenium clusters containing terminal Ru-CO groups. The diphenyltin ligand asymmetrically bridges the elongated Ru(2)-Ru(3) edge [Ru(2)–Sn(2) 2.6501(2) and Ru(3)–

Sn(2) 2.6926(3) Å], while the two Ph_3Sn ligands are bound to the Ru(1) [Ru(1)–Sn(1) 2.6607(2) Å] and Ru(3) [Ru(3)–Sn(3) 2.6854(3) Å] atoms at an equatorial coordination site. The ruthenium-tin bond distances observed in **2** are similar to those Ru-Sn distances reported in the literature for other structurally characterized Ru_3 and Ru_5 clusters containing an η^1-$SnPh_3$ ligand(s) [7b,9c,27]. Both hydride ligands were located crystallographically. One spans the dppm-bridged ruthenium-ruthenium edge, while the other is located within the Ru_3 core and is bound to all three ruthenium atoms. The DFT-optimized structure of **B** reproduces the important structural features found in **2**, and the charge data and WBIs are in keeping with the general feature of this cluster. Eq 1 shows the balanced reaction for the conversion of A→B which is highly exergonic by 165.8 kcal/mol. Solution spectroscopic data confirm that the solid-state structure persists in solution. The ^1H NMR spectrum displays two upfield resonances; a triplet at δ -10.21 (J_{PH} 14.6) and a singlet at δ -17.86 assigned to the edge-bridging (μ) and interstitial (μ_3) hydrides, respectively, in addition to other resonances for the methylene and phenyl protons. The $^{31}P\{^1H\}$ NMR spectrum shows two equal intensity doublets centered at δ 29.5 and 27.4 (J_{PP}77 Hz) for the inequivalent PPh_2 moieties of the dppm ligand. Again, the ^{119}Sn satellites were missing in both ^1H NMR and $^{31}P\{^1H\}$ NMR spectra of **2** even at 213 K (Figs. S13 and S15).

$$A + 2Ph_3SnH + 2Me_3NO \longrightarrow B + 2CO_2 + 2Me_3N + \text{benzene} \qquad \text{Eq 1}$$

The molecular structure of **3** is shown in Fig. 3, and the figure caption exhibits selected bond lengths and angles. The Ru(1)-Ru(2) and Ru(2)-Ru(3) bond distances of 3.0136(7) and 3.1724(8) Å, respectively, are on the long side of the ruthenium-ruthenium distances reported for polynuclear ruthenium clusters in the Cambridge Crystallographic Data Centre [28] but are consistent with the designation as Ru-Ru single bonds. The DFT-optimized structure of **C** (Fig. 1) is in accord with this, the presence of two Ru-Ru bonds being supported by the Wiberg bond indices of 0.33 and 0.27 for the dppm-bridged Ru-Ru bond and the elongated Ru-Ru bond that is tethered by the bridging Ph_2Sn groups, respectively. The Ru(1)···Ru(3) internuclear separation found in the X-ray structure is 5.411 Å which clearly precludes any significant bonding interaction, a feature reflected by the WBI of 0.02 computed for this particular bond (Table 1) and consistent with the total electron count of 50. The triphenyltin ligand [Sn(3)] is equatorially coordinated to the Ru(3) atom and the diphosphine ligand asymmetrically spans Ru(1)-Ru(2) edge [Ru(1)–P(1) 2.376(2) and

Ru(2)–P(2) 2.312(1) Å]. The $Ph_2Sn(2)$ ligand bridges the long Ru(2)-Ru(3) edge quite symmetrically [Ru(2)–Sn(2) 2.6351(7) and Ru(3)–Sn(2) 2.6518(7) Å], whilst the other $Ph_2Sn(1)$ moiety is bound to all three ruthenium atoms through the interior of the expanded metallic polyhedron. Although the Sn(1) is pentacoordinated, it donates two electrons to the cluster core akin to the quadruply bridged PhSn ligands in $[Ru_4(CO)_{12}(\mu_4\text{-}SnPh)_2]$ [2b,9a], $[Ru_4(CO)_{10}(\mu_4\text{-}SnPh)_2(\mu\text{-}SnPh_2)_2]$ [2b], $[Ru_4(CO)_9(\mu_4\text{-}SnPh)_2(\mu\text{-}SnPh_2)_3]$ [2b], $[Ru_4(CO)_8(\mu_4\text{-}SnPh)_2(\mu\text{-}SnPh_2)_4]$ [2b], $[Ru_5(CO)_{11}(C_6H_6)(\mu_4\text{-}SnPh)(\mu_3\text{-}CPh)]$ [7b] etc. which donates three electrons to the cluster core. Three relatively strong interactions exist between the Sn(1) center and the three ruthenium atoms based on the Wiberg bond indices that range from 0.56 to 0.59. We also computed the free energy change attendant in the conversion of **A**→**C**, and Eq 2 shows the balanced reaction that is exergonic by 37.0 kcal/mol.

$$A + 2Ph_3SnH \longrightarrow C + CO + 2(\text{benzene}) \qquad \text{Eq 2}$$

Place Figure 3 Here

While the hydride ligand was not located in the diffraction structure, it was assumed to span the Ru(1)–Sn(1) edge based on the disposition of the ligands about the cluster polyhedron and the NMR data recorded for the hydride. This premise was subsequently corroborated by DFT calculations that afforded species **C** as the hydride structure in concert with the solid-state structure. The ^1H NMR spectrum of **3** shows an upfield doublet of doublets for the lone hydride at δ -7.76 (J_{PH} 60.8, 6.8 Hz). The hydride resonance is deshielded slightly relative to those hydride resonances in clusters **1** and **2** reported here and other edge-bridging hydrides in ruthenium clusters whose chemical shifts are typically found from δ -10 to -20. The chemical shift of the hydride in **3** is close to the values reported for the agostic μ-silyl $Ru_2(CO)_5(SiTol_2H)(\mu\text{-}dppm)(\mu,\eta^2\text{-}HSiTol_2)$ and μ-silane $[Ru(CO)_2(SiTol_2H)]_2(\mu\text{-}dppm)(\mu,\eta^2\text{:}\eta^2\text{-}H_2SiTol_2)$ complexes [29, 30] that reveal a comparable hydride chemical shift at δ -8.87 and -8.84, respectively. The interaction that exists between the hydride ligand and the Ru_2-Sn_3 edge in **C** may be viewed within the context of an agostic-type association based on the Wiberg bond indices of 0.64 (Ru_2-H_1) and 0.09 (Sn_3-H_1). The hydride is more strongly bound to the ruthenium centre than the tin center, and this promotes a non-symmetrical bridging interaction of the hydride with the Ru-Sn edge in **C**. To probe this further, we have recorded and compared the ATR-FTIR spectra of **3** and Ph_3SnH. The Ph_3SnH shows an absorption at 1838 cm^{-1} due to a Sn-H stretching vibration in

its ATR-FTIR spectrum (Fig. S16). Although **3** also displays absorptions around 1850 cm^{-1} (Fig. S17), we could not assigned these absorptions to a Sn-H stretch unambiguously due to the presence of CO ligand stretching in the molecule in this same region. The $^{31}P\{^{1}H\}$ NMR spectrum of **3** exhibits a doublet at δ 41.9 (J_{PP} 68) and a triplet at δ 19.8 (J_{PP} 68) for the inequivalent PPh_2 moieties of the dppm ligand, the latter resonance also indicates that one of the phosphorus nuclei is coupled with hydride. Akin to **1** and **2**, we did not observe ^{119}Sn satellites in both ^{1}H NMR and $^{31}P\{^{1}H\}$ NMR spectra of **3** even at 213 K (Figs. S18 and S20).

Formation of **3** upon heating **2** results from both cleavage of a Sn-Ph bond (probably extruded as benzene) but also CO addition. As the yield of **3** is relatively low (31%) then presumably added CO results from degradation of a small amount of cluster **2**.

3. Summary and conclusions

The stepwise functionalization of $[Ru_3(CO)_{10}(\mu\text{-dppm})]$ by Ph_3SnH has been demonstrated under Me_3NO-promoted activation and direct thermolysis. The initial product $[Ru_3(CO)_9(SnPh_3)(\mu\text{-dppm})(\mu\text{-H})]$ (**1**) results from CO loss, coupled with Sn-H bond cleavage. This product reacts with further Ph_3SnH to give the dihydride cluster $[Ru_3(CO)_7(SnPh_3)_2(\mu\text{-}SnPh_2)(\mu\text{-dppm})(\mu\text{-H})(\mu_3\text{-H})]$ (**2**), resulting from the addition of a further two equivalents of Ph_3SnH and a secondary Sn-Ph bond scission. The cluster contains an edge-bridged hydride and a triply-bridged hydride that lies within the interior of an expanded metallic polyhedron, two of the ruthenium-ruthenium bonds being at the extreme end of distances attributed to ruthenium-ruthenium bonds. The final product, $[Ru_3(CO)_8(SnPh_3)(\mu\text{-}SnPh_2)(\mu_3\text{-}SnPh_2)(\mu\text{-dppm})(\mu_2\text{-H})]$ (**3**), is obtained upon thermolysis of **2** and is shown to contain two bridging Ph_2Sn ligands that help maintain the trimetallic framework of the product. Interestingly while it is the thermolysis product of **2** it also has one more CO ligand, thus the thermal rearrangement has led to an increase in the total electron count from 48 to 50, the reverse of the behaviour normally noted in low valent cluster chemistry. The structures of **1**-**3** have been established by spectroscopic and structural studies, and bonding aspects have been examined by DFT calculations. It is noteworthy that in all new Ru-Sn complexes the triruthenium core is maintained, highlighting once again the stabilising nature of the dppm ligand. A further point of note is our inability to isolate or identify any products with a Ru:Sn ratio of 3:2. These data suggest that the addition of the

second equivalent of Ph_3SnH activates the triruthenium centre to further oxidative addition (either Sn-H or Sn-C) and highlights the potential role of tin as a catalytic accelerant. The use of these new clusters as precursors for the stoichiometrically-controlled formation of RuSn nanoparticles and alloy precatalysts is on-going, the results of which will be presented in due course.

4. Experimental

4.1. General remarks

All reactions were carried under an inert atmosphere of nitrogen using standard Schlenk techniques unless otherwise stated. Reagent grade solvents were dried by the standard procedures and were freshly distilled prior to use. All ^{1}H and $^{31}P\{^{1}H\}$ NMR spectra were recorded on an Bruker Avance IIIHD (400 MHz) instrument. Solution IR spectra were recorded on a Shimadzu FTIR Prestige 21 spectrophotometer, and ATR-IR spectra were obtained on a Shimadzu IRTracer-100 instrument. Elemental analyses were performed by the Microanalytical Laboratory of Wazed Miah Science Research Centre at Jahangirnagar University. $[Ru_3(CO)_{12}]$ was purchased from Strem Chemical Inc. and used without further purification. Bis(diphenylphosphino)methane (dppm) and Ph_3SnH were purchased from Acros Chemicals Inc. and used as received. $[Ru_3(CO)_{10}(\mu\text{-dppm})]$ was prepared according to the published procedures [31]. Products were separated in the air on TLC plates coated with 0.25 mm layer of silica gel (HF_{254}-type 60, E. Merck, Germany).

4.2. Reaction of $[Ru_3(CO)_{10}(\mu\text{-dppm})]$ with Ph_3SnH at room temperature

A CH_2Cl_2 solution (10 mL) of Me_3NO (14 mg, 0.19 mmol) was added to a CH_2Cl_2 solution (20 mL) of $[Ru_3(CO)_{10}(\mu\text{-dppm})]$ (50 mg, 0.052 mmol) and Ph_3SnH (60 mg, 0.17 mmol) using a pressure equalizing dropping funnel over 15 min. The reaction solution was stirred for 2 h at room temperature, during which time the solution color changed from orange to red. The solution was then filtered through a short silica column (4 cm) to remove excess Me_3NO. The solvent was removed under reduced pressure and the residue chromatographed by TLC on silica gel. Elution with cyclohexane/CH_2Cl_2 (7:3, v/v) developed two major and two minor bands. The faster moving major band afforded $[Ru_3(CO)_7(SnPh_3)_2(\mu\text{-}SnPh_2)(\mu\text{-dppm})(\mu\text{-H})(\mu_3\text{-H})]$ (**2**) (23 mg, 24%) as red crystals while

the slower moving major band gave [$Ru_3(CO)_9(SnPh_3)(\mu\text{-dppm})(\mu\text{-H})$] (**1**) (30 mg, 45%) as yellow crystals after recrystallization from hexane/CH_2Cl_2 at 25 ^oC. The contents of the remaining minor bands were too small for characterization.

Analytical and spectroscopic data for **1**: Anal. Calcd for $C_{52}H_{38}O_9P_2Ru_3Sn$: C, 48.38; H, 2.97. Found: C, 48.85; H, 3.36%. IR (νCO, CH_2Cl_2): 2079w, 2043s, 2005vs, 1983sh, 1942sh, 1923w cm^{-1}. ^1H NMR (CD_2Cl_2): δ 7.82 (d, J 7.2, 1H), 6.40 (d, J 7.2, 1H), 7.60-7.07 (m, 33H), 4.55 (t, J_{PH} 10.8, 2H), -18.32 (d, J_{PH} 31.6, 1H). $^{31}P\{^1H\}$ NMR (CD_2Cl_2): δ 7.9 (br. s, 1P), 6.7 (br. s, 1P). FAB-MS: *m/z* 1291.

Analytical and spectroscopic data for **2**: Anal. Calcd for $C_{80}H_{64}O_7P_2Ru_3Sn_3$: C, 51.69; H, 3.47. Found: C, 52.05; H, 3.54%. IR (νCO, CH_2Cl_2): 2057m, 2026s, 2014vs, 1970s, 1942m cm^{-1}. ^1H NMR (CD_2Cl_2): δ 7.53 (m, 12H), 7.35-7.17 (m, 26H), 7.06-6.76 (m, 20H), 6.31 (m, 2H), 2.40 (m, 1H), 2.24 (m, 1H), -10.21 (t, J_{PH} 14.6, 1H), -17.79 (s, 1H).$^{31}P\{^1H\}$ NMR (CD_2Cl_2): δ 29.5 (d, J_{PP} 77, 1P), 27.4 (d, J_{PP} 77, 1P).

4.3. Reaction of [$Ru_3(CO)_{10}(\mu$-dppm)] with Ph_3SnH at 66 ^oC

A THF solution (30 mL) of [$Ru_3(CO)_{10}(\mu$-dppm)] (50 mg, 0.052 mmol) and Ph_3SnH (60 mg, 0.171 mmol) was heated to reflux for 90 min. The solvent was removed under reduced pressure and the residue chromatographically separated by TLC on silica gel. Elution with cyclohexane/CH_2Cl_2 (7:3, v/v) developed one major and several minor bands. The major band gave [$Ru_3(CO)_8(SnPh_3)(\mu\text{-}SnPh_2)_2(\mu_3\text{-}HSnPh_2)(\mu\text{-dppm})$] (**3**) (28 mg, 30%) as red crystals after recrystallization from hexane/CH_2Cl_2 at 4 ^oC, while the contents of minor bands were too small for characterization.

Analytical and spectroscopic data for **3**: Anal. Calcd for $C_{75}H_{58}O_8P_2Ru_3Sn_3$: C, 49.80; H, 3.23. Found: C, 50.33; H, 3.28%. IR (νCO, CH_2Cl_2): 2046w, 2030m, 2015m, 1983vs, 1925sh cm^{-1}. ^1H NMR (CD_2Cl_2): δ 7.76 (m, 3H), 7.57-7.49 (m, 10H), 7.34-7.02 (m, 35H), 6.74-6.67 (m, 7H),4.07 (t, J_{PH} 9.6, 2H), -7.76 (dd, J_{PH} 60.8, 6.8, 1H). $^{31}P\{^1H\}$ NMR (CD_2Cl_2): δ 41.9 (d, J_{PP} 68, 1P), 19.8 (t, J_{PP} 68, 1P).

*4.4. Conversion of **1** to **2***

To a CH_2Cl_2 solution (20 mL) of **1** (10 mg, 0.008 mmol) and Ph_3SnH (6 mg, 0.017 mmol) was added a CH_2Cl_2 solution (10 mL) of Me_3NO (2 mg, 0.027 mmol) using a pressure

equalizing dropping funnel. The mixture was stirred at room temperature for 2 h, and the product was isolated by chromatography, as described above, to give **2** (6 mg, 42%).

*4.5. Reaction of **1** with Ph_3SnH*

A THF solution (20 mL) of **1** (10 mg, 0.008 mmol) and Ph_3SnH (5 mg, 0.014 mmol) was heated to reflux for 2 h. Similar chromatographic separation and workup mentioned above gave **3** (5 mg, 36%).

*4.6. Conversion of **2** to **3***

A THF solution (15 mL) of **2** (10 mg, 0.0054 mmol) was refluxed for 1h. The solvent was removed under reduced pressure and the residue chromatographed by TLC on silica gel. Elution with cyclohexane/CH_2Cl_2 (7:3, v/v) developed three bands. The first band corresponded to unreacted **2** (3 mg). The second band isolated furnished **3** (3 mg, 31%) while the contents of the other band were too small for complete characterization.

4.7. Crystal structure determination

Single crystals of clusters **2** and **3** suitable for X-ray diffraction analysis were grown by slow diffusion of hexane into a CH_2Cl_2 solution containing each cluster. A suitable single crystal of **2** was mounted on an Agilent Super Nova dual diffractometer (Agilent Technologies Inc., Santa Clara, CA) using a Nylon Loop and the diffraction data were collected at 150(1) K using Cu-Kα radiation (λ = 1.54184). Unit cell determination, data reduction, and absorption corrections were carried out using CrysAlisPro [32]. The structure was solved with the ShelXS [33] structure solution program using Direct Methods and refined by full-matrix least-squares on the basis of F^2 using SHELXL 2013 [33] within the OLEX2 [34] graphical user interface. Non-hydrogen atoms were refined anisotropically, and hydrogen atoms (except those directly bonded to metals) were included using a riding model. One phenyl substituent on a tin atom [C47-C52] was disordered and refined over two sites with occupancies of 0.65:0.35. Some C-C distances within the minor component of the disordered phenyl group vary significantly from the ideal value of 1.395 Å**.** A suitable single crystal of **3** was mounted on a Bruker SMART APEX CCD diffractometer using glass fiber and the diffraction data were collected at 150(2) K using Mo-Kα radiation (λ = 0.71073). Data reduction and integration were carried out with SAINT+ and absorption corrections were

applied using the program SADABS [35]. Structures were solved by Direct methods and refined using full-matrix least-squares on F^2. All non-hydrogen atoms were refinedanisotropically. Hydrogen atoms were placed in the calculated positions and their thermal parameters linked to those of the atoms to which they were attached (riding model). The SHELXTL PLUS V6.10 program package was used for structure solution and refinement [36]. While PLATON reports solvent accessible voids in **3**, the largest residual electron density peak is only 1.062 $eÅ^{-3}$ and we attribute this to poor packing of the many phenyl groups in the structure. This is consistent with the fact that the density of **3** is *ca.* 0.1 gcm^{-3} less compared to **2**. Pertinent crystallographic parameters are given in Table 2.

4.8. Computational Methodology

The DFT calculations were carried out with the Gaussian 09 package of programs [37] using the B3LYP hybrid functional. This functional is comprised of Becke's three-parameter hybrid exchange functional (B3) [38] and the correlation functional of Lee, Yang, and Parr (LYP) [39]. The ruthenium and tin atoms were described with the Stuttgart-Dresden effective core potential and SDD basis set [40], and the 6-31G(d') basis set [41] was employed for the P, O, C, and H atoms.

The reported geometries for **A**-**C** were fully optimized, and the analytical Hessian was evaluated at each stationary point to confirm that the geometry was an energy minimum (no negative eigenvalues). Unscaled vibrational frequencies were used to make zero-point and thermal corrections to the electronic energies, and the resulting free energies are reported in kcal/molrelative to the specified standard. The geometry-optimized structures have been drawn with the *JIMP*2 molecular visualization and manipulation program [42].

Acknowledgments

This research has been partly sponsored by the Ministry of Science and Technology, Government of the People's Republic of Bangladesh. Part of this work was carried out by S. E. K. at the University of Göttingen. S. E. K. gratefully acknowledges the von Humboldt Foundation for a Fellowship to spend time at the University of Göttingen. M. G. R. thanks the Robert A. Welch Foundation (grant B-1093) for financial support and acknowledges computational resources through UNT's High-Performance Computing Services and

CASCaM. We also thank Prof. Michael B. Hall (TAMU) for providing us a copy of his *JIMP2* program.

Supplementary data

Electronic supplementary information (ESI) contains IR, NMR, VT NMR spectra and atomic coordinates of DFT-optimized structures. CCDC 1511020 and CCDC 1506077 contain supplementary crystallographic data for **2** and **3** respectively. These data may be obtained free of charge from The Cambridge Crystallographic Data Center via www.ccdc.cam.ac.uk/data_request/cif.

References

[1] (a) P. Braunstein, J. Rosé, In Metal Clusters in Chemistry, P. Braunstein, L.A. Oro, P.R. Raithby, Eds., Wiley-VCH: Weinheim, Germany, (1999), Vol. 2, Chapter 2.2, pp 616-677;
(b) P. Braunstein, J. Rosé, In Catalysis by Di- and Polynuclear Metal Cluster Complexes, R.D. Adams, F.A. Cotton, Eds., Wiley-VCH: New York, (1998), Chapter 13.

[2] (a) R.D. Adams, E. Trufan, Phil. Trans. R. Soc. A 368 (2010) 1473-1493;
(b) R.D. Adams, E.M. Boswell, B. Captain, A.B. Hungria, P.A. Midgley, R. Raja, J.M. Thomas, Angew. Chem. Int. Ed. 46 (2007) 8182-8185;
(c) A.B. Hungria, R. Raja, R.D. Adams, B. Captain, J.M. Thomas, P.A. Midgley, V. Golvenko, B.F.G. Johnson, Angew. Chem. Int. Ed. 45 (2006) 4782-4785.

[3] (a) S. Hermans, R. Raja, J.M. Thomas, B.F.G. Johnson, G. Sankar, D. Gleeson, Angew. Chem. Int. Ed. 40 (2001) 1211-1215;
(b) J.M. Thomas, B.F.G. Johnson, R. Raja, G. Sankar, P.A. Midgley, Acc. Chem. Res. 36 (2003) 20-30.

[4] (a) R.D. Adams, D.A. Blom, B. Captain, R. Raja, J.M. Thomas, E. Trufan, Langmuir 24 (2008) 9223-9226;
(b) J.M. Thomas, R.D. Adams, E.M. Boswell, B. Captain, H. Grönbeck, R. Raja, Faraday Disc. 138 (2008) 301-315.

[5] (a) R. Burch, J. Catal. 71 (1981) 348-359;
(b) R. Burch, L.C. Garla, J. Catal. 71 (1981) 360-372;
(c) T. Fujikawa, F.H. Ribeiro, G.A. Somorjai, J. Catal. 178 (1998) 58-65;
(d) Y.-K. Park, F.H. Ribeiro, G.A. Somorjai, J. Catal. 178 (1998) 66-75;
(e) R.D. Cortright, J.A. Dumesic, J. Catal. 148 (1997) 771-778;
(f) F.M. Dautzenberg, J.N. Helle, P. Biolen, W.M.H. Sachtler, J. Catal. 63 (1980) 119-128;
(g) J.W. Shabaker, D.A. Simonetti, R.D. Cortright, J.A. Dumesic, J. Catal. 231 (2005) 67-76;
(h) R. Srinivasan, B.H. Davis, Platinum Met. Rev. 36 (1992) 151-163;
(i) F. Epron, C. Carnevillier, P. Marecot, Appl. Catal. 295 (2005) 157-169.

[6] (a) G.W. Huber, J.W. Shabaker, J.A. Dumesic, Science 300 (2003) 2075-2077;
(b) M. Guidotti, V. Dal Aanto, A. Gallo, E. Gianotti, G. Peli, R. Psaro, L. Sordelli, Catal. Lett. 112 (2006) 89-95;
(c) R.D. Cortright, J.M. Hill, J.A. Dumesic, Catal. Today 55 (2000) 213-223;
(d) B.F.G. Johnson, S.A. Raynor, D.B. Brown, D.S. Shephard, T. Mashmeyer, J.M. Thomas, S. Hermans, R. Raja, G. Sankar, J. Mol. Catal. A: Chem. 182-183 (2002) 89-97;
(e) S. Hermans, B.F.G. Johnson, Chem. Commun. (2000) 1955-1956.

[7] (a) R.D. Adams, B. Captain, W. Fu, M.D. Smith, Inorg. Chem. 41 (2002) 2302-2303;
(b) R.D. Adams, B. Captain, W. Fu, M.D. Smith, Inorg. Chem. 41 (2002) 5593-5601;
(c) R.D. Adams, B. Captain, J.L. Smith, Jr, M.B. Hall, C.L. Beddie, C.E. Webster, Inorg. Chem. 43 (2004) 7576-7578;
(d) R.D. Adams, B. Captain, L. Zhu, Organometallics 25 (2006) 2049-2054.

[8] (a) R.D. Adams, B. Captain, L. Zhu, Inorg. Chem. 44 (2005) 6623-6631;
(b) R.D. Adams, E. Trufan, Organometallics 27 (2008) 4108-4115;
(c) R.D. Adams, B. Captain, M.B. Hall, E. Trufan, X. Yang, J. Am. Chem. Soc. 129 (2007) 12328-12340;
(d) R.D. Adams, E.M. Boswell, B. Captain, M.A. Patel, Inorg. Chem. 46 (2007) 533-540.

[9] (a) R.D. Adams, Y. Kan, V. Rassolov, Q. Zhang, J. Organomet. Chem. 730 (2013) 20-31;
(b) R.D. Adams, B. Captain, L. Zhu, Organometallics 25 (2006) 4183-4187;
(c) R.D. Adams, B. Captain, E. Trufan, J. Organomet. Chem. 693 (2008) 3593-3602.

[10] (a) J.A. Cabeza, I. del Rio, J.M. Fernandez-Colinas, M.G. Sanchez-Vega, Organometallics 28 (2009) 1243-1247;
(b) C. Bois, J.A. Cabeza, R.J. Franco, V. Riera, E. Saborit, J. Organomet. Chem. 564 (1998) 201-207;
(c) J.A. Cabeza, I. del Rio, V. Riera, Inorg. Chim. Acta 268 (1998) 131-133;
(d) J.A. Cabeza, R.J. Franco, V. Riera, S. Garcia-Granda, J.F. Van der Maelen, Organometallics 14 (1995) 3342-3348.

[11] (a) J.A. Cabeza, R.J. Franco, V. Riera, Inorg. Chem. 33 (1994) 5952-5954;
(b) J.A. Cabeza, R.J. Franco, A. Llamazares, V. Riera, C. Bois, Y. Jeannin, Inorg. Chem. 32 (1993) 4640-4642;
(c) J.A. Cabeza, S. Garcia-Granda, A. Llamazares, V. Riera, J.F. Van der Maelen, Organometallics 12 (1993) 157-163;
(d) J.A. Cabeza, A. Llamazares, V. Riera, S. Triki, L. Ouahab, Organometallics 11 (1992) 3334-3339.

[12] J.D. Cotton, S.A.R. Knox, F.G.A. Stone, J. Chem. Soc. Chem. Commun. (1967) 965-966.

[13] (a) M.R. Hassan, G. Hogarth, G.M.G. Hossain, S.E. Kabir, A.K. Raha, M.S. Saha, D.A. Tocher, Organometallics 26 (2007) 6473-6480;
(b) J.C. Sarker, K.M. Uddin, M.S. Rahman, S. Ghosh, T.A. Siddiquee, D.A. Tocher, M.G. Richmond, G. Hogarth, S.E. Kabir, Inorg. Chim. Acta 409 (2014) 320-329;
(c) S.E. Kabir, G. Hogarth, Coord. Chem. Rev. 253 (2009) 1285-1315.

[14] (a) D.J. Cardin, M.F. Lappert, J. Chem. Soc. Chem. Commun. (1966) 506-506;
(b) D.J. Cardin, S.A. Keppie, M.F. Lappert, J. Chem. Soc. A (1970) 2594-2598;
(c) J.L. Greàt-Morales, J.M. Fernàndez-G, Organometallics 23 (2004) 3840-3846.

[15] (a) S.E. Kabir, A.K. Raha, M.R. Hassan, B.K. Nicholson, E. Rosenberg, A. Sharmin, L. Salassa, DaltonTrans. 32 (2008) 4212-4219;
(b) S. Ghosh, R. Pervin, A.K. Raha, S.E. Kabir, B.K. Nicholson, Inorg. Chim. Acta 362 (2009) 4226-4230.
(c) A.K. Raha, S. Ghosh, I. Hossain, S.E. Kabir, B.K. Nicholson, G. Hogarth, L. Salassa, J. Organomet. Chem. 696 (2011) 2153-2160.

[16] (a) L. Alvarez-Rodriguez, J.A. Cabeza, P. Garcia-Alvarez, D. Polo, Coord. Chem. Rev. 300 (2015) 1-28;
(b) J.A. Cabeza, P. Garcia-Alvarez, D. Polo, Inorg. Chem. 51 (2012) 2569-2576;
(c) J.A. Cabeza, P. Garcia-Alvarez, D. Polo, Dalton Trans. 42 (2013) 1329-1332.

[17] A.K. Raha, S. Ghosh, S.E. Kabir, B.K. Nicholson, D.A. Tocher, J. Organomet. Chem. 694 (2009) 752-756.

[18] M.R. Haque, M.J. Hossain, A. Rahaman, S. Ghosh, S.E. Kabir, G. Hogarth, D.A. Tocher, J. Organomet. Chem. 812 (2016) 240-246.

[19] A.J. Deeming, M.M. Hassan, S.E. Kabir, E. Nordlander, D.A. Tocher, Dalton Trans. (2004) 3709-3714.

[20] (a) L. Yang, V.N. Nesterov, X. Wang, M.G. Richmond, J. Clust. Sci. 23 (2012) 685-702;

(b) C.-H. Lin, V.N. Nesterov, M.G. Richmond, J. Organomet. Chem. 744 (2013) 24-34.

[21] Here we have used a van der Waals radius of 2.07 Å for ruthenium, as taken from the Periodic Table of Elements: Los Alamos National Laboratory (http://periodic.lanl.gov/73).

[22] D.M. Mingos, D.J. Wales, Introduction to Cluster Chemistry, Prentice Hall, Englewood Cliffs, NJ, 1990.

[23] R.D. Adams, Z. Li, J.-C. Lii, W. Wu, Inorg. Chem. 31 (1992) 3445-3450.

[24] A.J. Deeming, K.I. Hardcastle, M. Karim, Inorg. Chem. 31 (1992) 4792-4796.

[25] M. Bown, J.M. Waters, J. Am. Chem. Soc. 112 (1992) 2442-2443.

[26] M.P. Cifuentes, T.P. Jeynes, M.G. Humphrey, B.W. Skelton, A.H. White, J. Chem. Soc. Dalton Trans. (1994) 925-930.

[27] J.A. Cabeza, I. del Río, J.M. Fernández-Colinas, M.G. Sánchez-Vega, Organometallics 28 (2009) 1243-1247.

[28] For dppm-bridged Ru-Ru bond lengths of comparable magnitude, see: (a) C.E. Housecroft, A.L. Rheingold, A. Waller, G.P.A. Yap, J. Organomet. Chem. 565 (1998) 105-114;

(b) H.-C. Böttcher, M. Graf, Merzweiler, C. Wagner, Z. Anorg. Allg. Chem. 627 (2001) 2657-2662;

(c) M.I. Hyder, S.E. Kabir, M.A. Miah, T.A. Siddiquee, G.M.G. Hossain, Polyhedron 24 (2005) 1471-1477;

(d) K.-B. Shui, W.-N. Guo, T.-J. Chan, J.-C. Wang, L.-S. Liou, S.-M. Peng, M.-C. Cheng, Organometallics 14 (1995) 1732-1738.

[29] H. Hashimoto, Y. Hayashi, I. Aratani, C. Kabuto, M. Kira, Organometallics 21 (2002) 1534-1536.

[30] For additional reports of agostic Si-H/Sn-H interactions with a metal center, see: (a) U. Schubert, E. Kunz, B. Harkers, J. Willnecker, J. Meyer, J. Am. Chem. Soc. 111 (1989) 2572-2574;
(b) J.C. Sarker, K. M. Uddin, M.S. Rahman, S. Ghosh, T.A. Siddiquee, D.A. Tocher, M.G. Richmond, G. Hogarth, S.E. Kabir, Inorg. Chim. Acta 409 (2014) 320-329;
(c) A. Koppaka, V. Yempally, L. Zhu, G.C. Fortman, M. Temprado, C.D. Hoff, B. Captain, Inorg. Chem. 55 (2015) 307-321;
(d) S.M. Rummelt, K. Radkowski, D.-A. Rosca, A. Fürstner, J. Am. Chem. Soc. 137 (2015) 5506-5519.

[31] M.I. Bruce, B.K. Nicholson, M.L. Williams, Inorg. Synth. 26 (1990) 265-280.

[32] CrysAlisPro; Oxford Diffraction: Yarnton, England (2015).

[33] G.M. Sheldrick, ActaCryst. A 64 (2008) 112-122.

[34] O.V. Dolomanov, L.J. Bourhis, R.J. Gildea, J.A.K. Howard, H. Puschmann, J. Appl. Cryst. 42 (2009) 339-341.

[35] SMART and SAINT software for CCD diffractometers, version 6.1, Madison, WI (2000).

[36] G.M. Sheldrick, SHELXTL PLUS, version 6.10, Bruker AXS, Madison, W1 (2000).

[37] M.J. Frisch, G.W. Trucks, H.B. Schlegel, G.E. Scuseria, M.A. Robb, J.R. Cheeseman, G. Scalmani, V. Barone, B. Mennucci, G.A. Petersson, H. Nakatsuji, M. Caricato, X. Li, H.P. Hratchian, A.F. Izmaylov, J. Bloino, G. Zheng, J.L. Sonnenberg, M. Hada, M. Ehara, K. Toyota, R. Fukuda, J. Hasegawa, M. Ishida, T. Nakajima, Y. Honda, O. Kitao, H. Nakai, T. Vreven, J.A. Montgomery, Jr., J.E. Peralta, F. Ogliaro, M. Bearpark, J.J.. Heyd, E. Brothers, K.N. Kudin, V. N. Staroverov, R. Kobayashi, J. Normand, K. Raghavachari, A. Rendell, J.C. Burant, S.S. Iyengar, J. Tomasi, M. Cossi, N. Rega, J.M. Millam, M. Klene, J.E. Knox, J.B. Cross, V. Bakken, C. Adamo, J. Jaramillo, R. Gomperts, R.E. Stratmann, O. Yazyev, A.J. Austin, R. Cammi, C. Pomelli, J.W. Ochterski, R.L. Martin, K. Morokuma, V.G. Zakrzewski, G.A. Voth, P. Salvador, J.J. Dannenberg, S. Dapprich, A.D. Daniels, O. Farkas, J.B. Foresman, J.V. Ortiz, J. Cioslowski, D.J. Fox, Gaussian 09, Revision A.02, Gaussian, Inc., Wallingford CT, 2009.

[38] A.D. Becke, J. Chem. Phys. 98 (1993) 5648-5652.

[39] C. Lee, W. Yang, R.G. Parr, Phys. Rev. B 37 (1988) 785-789.

[40] (a) M. Dolg, U. Wedig, H. Stoll, H. Preuss, J. Chem. Phys. 86 (1987) 866-872;
(b) S.P. Walch, C.W. Bauschlicher, J. Chem. Phys. 78 (1983) 4597-4605.

[41] (a) G.A. Petersson, A. Bennett, T.G. Tensfeldt, M.A. Al-Laham, W.A. Shirley, J. Mantzaris, J. Chem. Phys. 89 (1988) 2193-2218;
(b) G.A. Petersson, M.A. Al-Laham, J. Chem. Phys. 94 (1991) 6081-6090.

[42] (a) JIMP2, version 0.091, a free program for the visualization and manipulation of molecules: M.B. Hall, R.F. Fenske, Inorg. Chem. 11 (1972) 768-775;
(b) J. Manson, C.E. Webster, M.B. Hall, Texas A&M University, College Station, TX, (2006): http://www.chem.tamu.edu/jimp2/index.html

Table 1

Selected natural charges and Wiberg bond indices for the DFT-optimized species **A**-**C**[a]

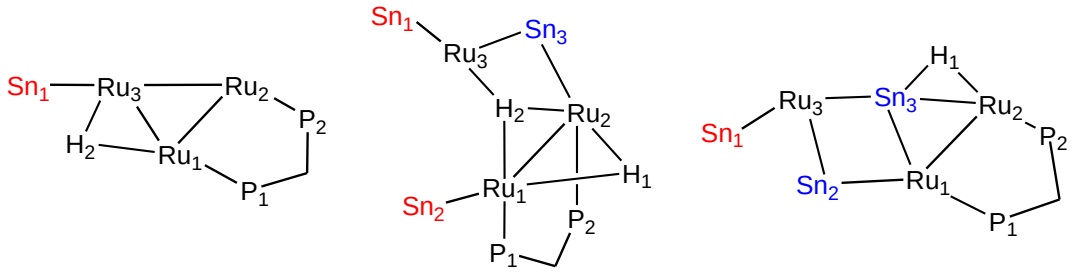

A **B** **C**

Natural Charge

species	Ru_1	Ru_2	Ru_3	P_1	P_2	Sn_1	Sn_2	Sn_3	H_1	H_2
A	-1.52	-1.40	-1.58	1.36	1.31	1.79				0.13
B	-1.55	-1.52	-1.95	1.30	1.30	1.81	1.83	1.73	0.08	0.10
C	-1.93	-1.62	-2.16	1.34	1.29	1.82	1.75	1.76	0.11	

Wiberg bond indices[b]

species	Ru_1-Ru_2	Ru_2-Ru_3	Ru_1-Ru_3	Ru_1-Sn_2	Ru_3-Sn_2	Ru_1-Sn_3	Ru_2-Sn_3	Ru_3-Sn_3	Ru_1-H_2	Ru_2-H_2	Ru_3-H_2	Sn_3-H_1	Ru_1-H_1	Ru_2-H_1
A	0.37	0.40	0.23						0.42		0.32			
B	0.22	0.16	0.12	0.62			0.55	0.59	0.25	0.26	0.30		0.43	0.34
C	0.33	0.02	0.27	0.56	0.59	0.58	0.19	0.39				0.09	0.02	0.64

[a]Atom numbers based on the numbering scheme for the different Ru_3 clusters (**A**-left; **B**-center; **C**-right) examined in this study. The depicted Sn and Sn atoms represent Ph_3Sn and Ph_2Sn moieties, respectively. [b]The mean WBI for the Ru_3-Sn_1 vectors is 0.59.

Table 2

Crystallographic and structure refinement data for **2** and **3**

Compound	**2**	**3**
Empirical formula	$C_{80}H_{64}O_7P_2Ru_3Sn_3$	$C_{75}H_{58}O_8P_2Ru_3Sn_3$
Formula weight	1858.53	1808.43
Temperature (K)	150	150(2)
Wavelength (Å)	1.54184	0.71073
Crystal system	Monoclinic	Triclinic
Space group	*P* $2_1/n$	*P*-1
Unit cell dimensions		
a (Å)	11.83579(7)	11.527(3)
b (Å)	33.90437(19)	16.216(4)
c (Å)	17.79811(12)	19.938(5)
α (°)	90	85.646(4)
β (°)	90.5029(6)	83.389(4)
γ (°)	90	86.554(4)
Volume (Å^3)	7141.84(8)	3686.4(14)
Z	4	2
Density (calculated) (g/cm^3)	1.728	1.629
Absorption coefficient (mm^{-1})	14.082	1.694
F(000)	3648.0	1768
Crystal size (mm^3)	0.17 × 0.11 × 0.08	0.22 × 0.18 × 0.16
2θ range for data collection (°)	7.202 to 148.258	4.82 to 56.94
Index ranges	$-14 \le h \ge 14$	$-15 \le h \ge 15$
	$-41 \le k \ge 42$	$-21 \le k \ge 21$
	$-22 \le l \ge 22$	$-25 \le l \ge 26$
Reflections collected	128435	31011
Independent reflections	14430 [R_{int} = 0.0381]	16520 [R_{int} = 0.0435]
Data/restraints/parameters	14430 / 0 / 910	16520 / 0 / 820
Goodness-of-fit on F^2	1.121	0.880
Final *R* indices [$I>2\sigma(I)$]	R_1 = 0.0234,	R_1 = 0.0422,
	wR_2 = 0.0513	wR_2 = 0.0855
R indices (all data)	R_1 = 0.0249,	R_1 = 0.0817,
	wR_2 = 0.0520	wR_2 = 0.0917
Largest diff. peak and hole (eÅ^{-3})	0.98 and −0.73	1.062 and −0.625

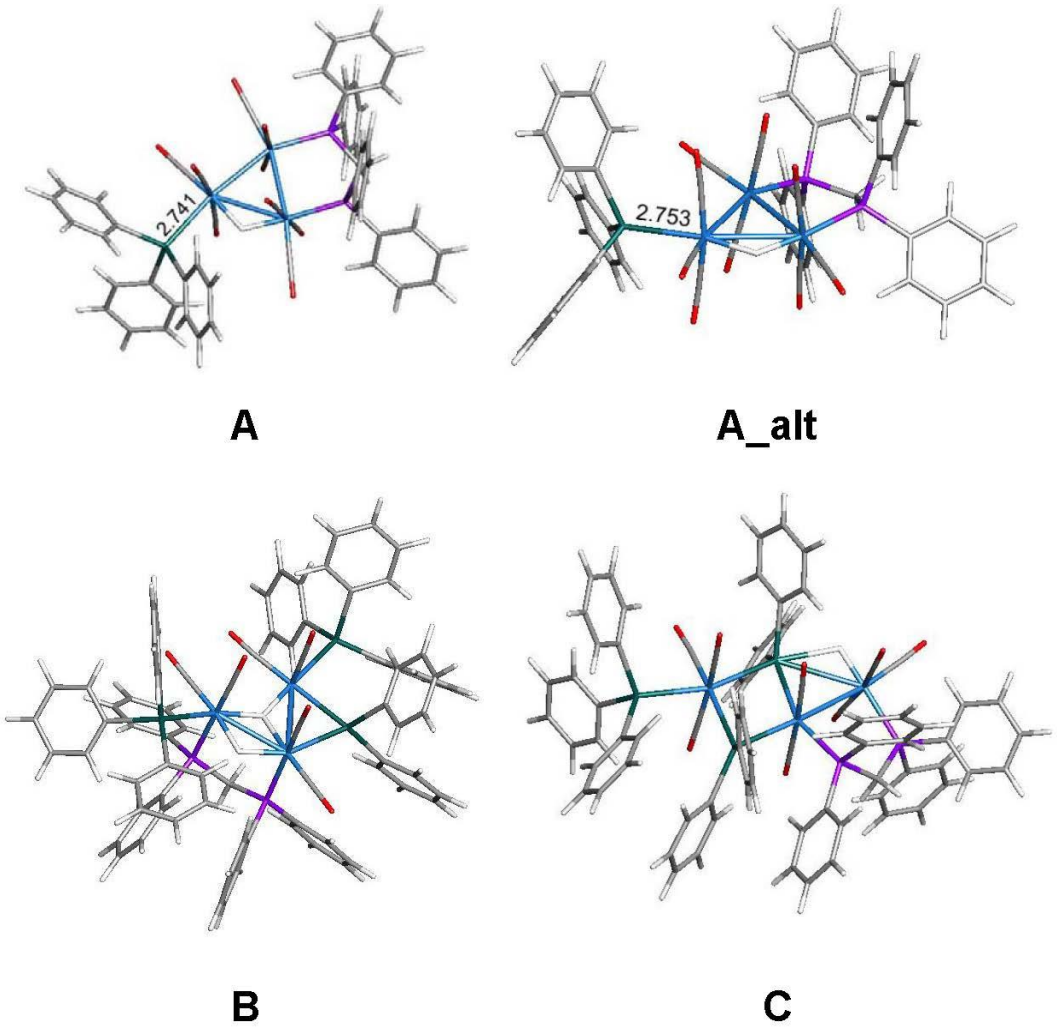

Fig. 1. DFT-optimized structures for the isomers of $[Ru_3(CO)_9(SnPh_3)(\mu\text{-dppm})(\mu\text{-H})]$ (**A** and **A_alt**), and the clusters $[Ru_3(CO)_7(SnPh_3)_2(\mu\text{-}SnPh_2)(\mu\text{-dppm})(\mu\text{-H})(\mu_3\text{-H})]$ (**B**), and $[Ru_3(CO)_8(SnPh_3)(\mu\text{-}SnPh_2)(\mu_3\text{-}SnPh_2)(\mu\text{-dppm})(\mu\text{-H})]$ (**C**).

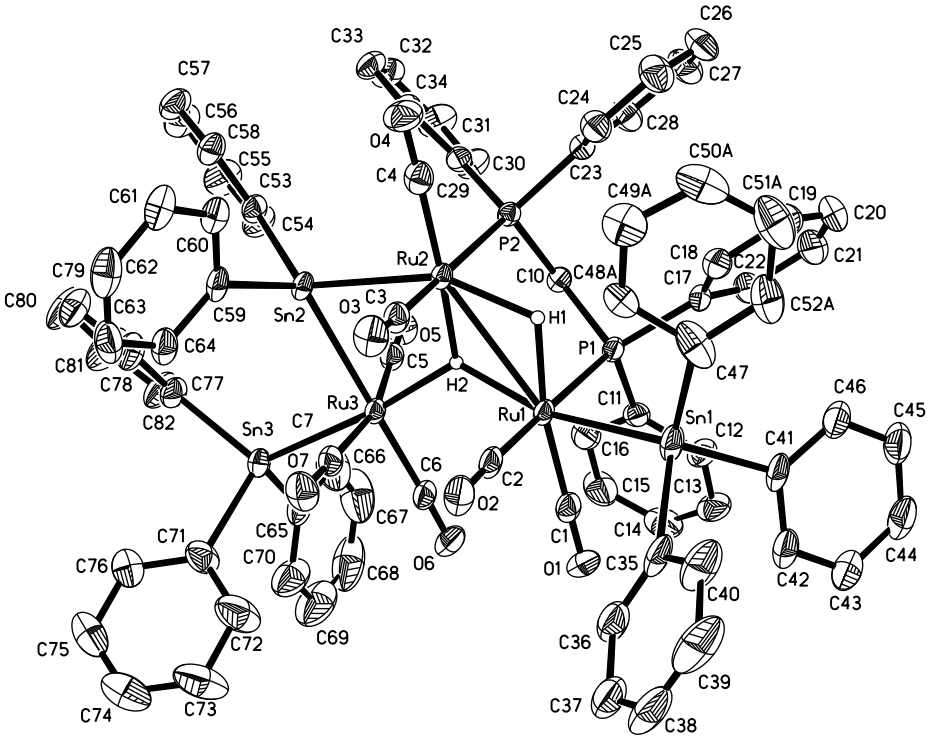

Fig. 2. ORTEP diagram of the molecular structure of $[Ru_3(CO)_7(SnPh_3)_2(\mu\text{-}SnPh_2)(\mu\text{-}dppm)(\mu\text{-}H)(\mu_3\text{-}H)]$ (**2**), showing 50% probability thermal ellipsoids. Hydrogen atoms except those directly bonded to ruthenium are omitted for clarity. Selected bond lengths (Å) and angles (°): Ru(1)–Ru(2) 2.9439(3), Ru(2)-Ru(3) 3.2355(5), Ru(1)-Ru(3) 3.3992(7), Ru(1)–Sn(1) 2.6607(2), Ru(2)–Sn(2) 2.6501(2), Ru(3)–Sn(2) 2.6926(3), Ru(3)–Sn(3) 2.6854(3), Ru(1)–P(1) 2.3825(7), Ru(2)–P(2) 2.3996(6), Sn(1)–Ru(1)–Ru(2) 124.686(9), P(1)–Ru(1)–Sn(1) 94.05(2), P(1)–Ru(1)–Ru(2) 90.89(2), P(2)–Ru(2)–Sn(2) 102.91(2), Ru(2)–Sn(2)–Ru(3) 74.537(7), Sn(2)–Ru(3)–Sn(3) 94.045(8), Sn(2)–Ru(2)–Ru(1) 119.208(8).

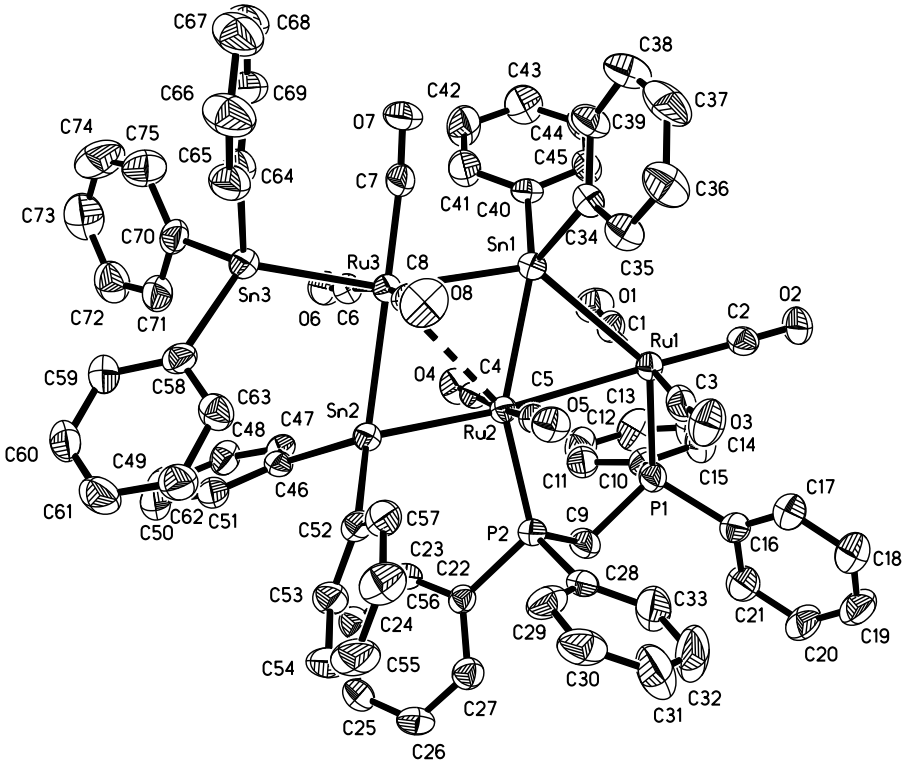

Fig. 3. ORTEP diagram of the molecular structure of $[Ru_3(CO)_8(SnPh_3)(\mu\text{-}SnPh_2)_2(\mu_3\text{-}HSnPh_2)(\mu\text{-}dppm)]$ (**3**), showing 50% probability thermal ellipsoids. Hydrogen atoms are omitted for clarity. Selected bond lengths (Å) and angles (°): Ru(1)–Ru(2) 3.0136(7), Ru(2)–Ru(3) 3.1724(8), Ru(1)–Sn(1) 3.0640(8), Ru(2)–Sn(1) 2.6284(7), Ru(2)–Sn(1) 2.6284(7), Ru(3)–Sn(1) 2.7953(7), Ru(2)–Sn(2) 2.6351(7),Ru(3)–Sn(2) 2.6518(7), Ru(3)–Sn(3) 2.6570(7), Ru(1)–P(1) 2.376(2), Ru(2)–P(2) 2.312(1), Ru(1)–Sn(1)–Ru(2) 63.39(2), Ru(1)–Sn(1)–Ru(3) 134.84(2),Sn(1)–Ru(1)–Ru(2) 51.25(2),Sn(1)–Ru(2)–Ru(1) 65.38(2), Sn(1)–Ru(2)–Sn(2) 110.08(2),Sn(1)–Ru(3)–Sn(2) 104.70(2), Ru(2)–Sn(1)–Ru(3) 71.50(2), Ru(2)–Sn(2)–Ru(3) 73.72(2), Sn(1)–Ru(3)–Sn(3) 162.68(2), Sn(2)–Ru(3)–Sn(3) 92.60(2), Sn(2)–Ru(2)–Ru(1) 175.06(2), P(1)–Ru(1)–Ru(2) 89.15(4), P(2)–Ru(2)–Sn(2) 95.11(4).

Graphical Abstract

Mixed Main Group Transition Metal Clusters: Reactions of $[Ru_3(CO)_{10}(\mu\text{-dppm})]$ with Ph_3SnH

Md. Mehedi Mahabub Khan [a], Shishir Ghosh [a], Graeme Hogarth [b], Derek A. Tocher [c], Michael G. Richmond [d], Shariff E. Kabir [a, e, *], Herbert W. Roesky [e, *]

The structure and bonding of several dppm-ligated ruthenium-tin clusters prepared from the reactions between $[Ru_3(CO)_{10}(\mu\text{-dppm})]$ and Ph_3SnH have been examined.